Robotica: (2020) volume 38, pp. 2173–2188. © Cambridge University Press 2020
doi:10.1017/S0263574720000028

A Systematic Approach for Accuracy Design of Lower-Mobility Parallel Mechanism

Wenjie Tian†‡*, Ziqian Shen†, Dongpo Lv†, and Fuwen Yin‡

†*School of Marine Science and Technology, Tianjin University, Tianjin 300072, China.*
E-mails: 136597810@qq.com, lvdongpo@tju.edu.cn
‡*Key Laboratory of Mechanism Theory and Equipment Design of Ministry of Education, Tianjin University, Tianjin 300072, China. E-mail: yinfw@tju.edu.cn*

(Accepted December 27, 2019. First published online: February 5, 2020)

SUMMARY
Geometric accuracy is a critical performance factor for parallel robots, and regardless of error compensation, accuracy design or tolerance allocation is another way to ensure the pose accuracy of a robot at design stage. A general method of both geometric error modeling and accuracy design of lower-mobility parallel mechanisms is presented. First, a general approach for error modeling of lower-mobility parallel mechanism is proposed based on screw theory, and then the geometric errors affecting the compensatable and uncompensatable accuracy of the end-effector are separated using the properties of dual vector space. The pose error aroused by compensatable geometric errors can be compensated via kinematic calibration, while the uncompensatable geometric errors should be minimized during the manufacturing and assembly processes. Based on that, the tolerance allocation method is presented, giving each uncompensatable geometric error a proper tolerance by the use of reliability theory. Compared with the traditional tolerance allocation method, the advantages of the proposed method are as follows: the number of geometric errors to be allocated is greatly reduced; the results of serialized tolerance allocation can be obtained according to different reliability indices of pose accuracy of end-effector for designers to choose; on the premise of guaranteeing the same pose accuracy of end-effector, the allocated tolerances are loose and easy to realize. Finally, the proposed methods are successfully applied to an R(2-RPS&RP)&UPS lower-mobility parallel robot, and the effectiveness and practicability of the proposed method are verified.

KEYWORDS: Lower-mobility parallel mechanism; Error modeling; Accuracy design; Tolerance allocation; Reliability theory.

1. Introduction

In recent years, there has been a high demand for large, accurate parts for several "high-growth" industries such as aviation, railways, and shipping.[1] Traditionally, a large gantry 5-axis machine tool is used, which weighs several tons and covers a large area. Using one or more machining modules, which can move along a long trajectory that forms the basis of the manufacturing system, is an innovative approach: each module is a parallel or hybrid robot. Compared to conventional serial industrial robots, lower-mobility parallel mechanisms have advantages in many aspects, such as accuracy, rigidity, high workspace/footprint ratio, dynamic response, and flexibility. Based on that, some parallel kinematic robots have proved useful, for instance, the Ecospeed with the Sprint Z3 head[2] has been

* Corresponding author. E-mail: wenjietian@tju.edu.cn

used for manufacturing of large aluminum alloy components, and the Tricept[3] and the Exechon[4] have been used for high-speed milling, drilling, deburring, and other manipulations, either as a stand-alone machine or as part of a movable robotized cell.

Geometric accuracy is a critical performance factor for lower-mobility parallel mechanisms, especially when relatively high precision is one of the fundamental demands.[5] Regardless of kinematic calibration,[6,7] a process when estimating the actual kinematics such that the inverse kinematic model stored in the computerized numerical control controller can be modified, accuracy design is another way to ensure the pose accuracy of robot in the design stage. Tolerance allocation is a process of determining which tolerances should be allocated tight values and how much tolerance is allocated; it depends mainly on the experience of the designer; therefore, how to obtain a more reasonable allocation or to provide designers with informative guidelines for accuracy design is a challenging issue.[8]

Geometric error modeling is the basis of accuracy design, involving a mapping between the pose error of the end-effector and geometric source errors. In previous years, there have been several studies undertaken on error modeling. The most extensive approach is to use a homogeneous transformation matrix or Denavit–Hartenberg (D–H) transformation matrix to describe the coordinate transformation between each rigid body frame and its reference coordinate system,[9,10] which is based on rigid body kinematics. The vector loop method,[11,12] product of exponentials (POE) method,[13,14] and screw method[15–17] are some other useful tools for such error modeling. Most recently, a generalized Jacobian method has been approved for describing unexpected small deviations from the ideal motions of the end-effector[18] and an error modeling approach is proposed for distinguishing the source errors affecting compensatable pose errors from those affecting uncompensatable ones.[19] Inspired by this idea, a new method for error modeling of lower-mobility parallel mechanisms will be introduced here, such that appropriate measures can be taken for accuracy improvement via accuracy design, manufacture, and assembly, as well as by kinematic calibration.

Tolerance allocation is an important part of mechanical design of industrial robot. Tighter tolerances often result in higher-quality components and better performance in robotics system, but unnecessarily tight tolerances can lead to excessive manufacturing costs for specific applications.[5] Minimizing manufacturing cost, which is constrained by specified allowable pose accuracy, manufacturing feasibility, etc., is an oft-used approach for dealing with tolerance allocation. Building upon statistical or worst-case error models, several cost-tolerance functions for minimization and algorithms for improving computational efficiency have been proposed;[20–25] however, for these traditional methods, all geometric errors are taken into consideration; thus, the allocated tolerances are often too tight to be realized in actual engineering practice; therefore, we propose a new method for tolerance allocation. As mentioned above, we can divide all geometric errors into two types: those that only influence compensatable pose accuracy and those that influence uncompensatable pose accuracy. Apparently, the latter are more significant so more attention should be paid to them in the process of tolerance design; however, how to divide the geometric errors into the above two groups and how to assign appropriate weights thereto for tolerance design remain unsolved problems.

After Section 1 has briefly addressed current challenges in geometric error modeling and accuracy design of lower-mobility parallel mechanisms, Section 2 proposes an error modeling approach for lower-mobility parallel mechanism, which allows the geometric errors affecting the compensatable and uncompensatable pose accuracy of the end-effector to be identified. In Section 3, a tolerance allocation approach is proposed based on the reliability theory. Finally, the proposed methods are applied to a parallel mechanism, and Monte Carlo simulation (MCS) verifies their effectiveness in Section 4, before conclusions are drawn in Section 5.

2. Geometric Error Modeling and Error Separation

In this section, the linear map between the pose error twist of the platform and all possible geometric errors in joints and links will be formulated using screw theory. Geometric errors affecting the compensatable and uncompensatable pose accuracy of the parallel mechanism will then be separated, thus providing guidance for designers with which they can improve accuracy through appropriate approaches, that is, component tolerance allocation in design, manufacturing and assembly processes, and kinematic calibration.

Figure 1 shows an f-degree of freedom (DOF) parallel mechanism composed of a base and a platform, connected by l limbs. Here, we assume that the ith limb consists of $(n_i + 1)$ links which are serially connected by n_i $(i = 1, 2, \cdots, l)$ 1-DOF joints, with at most one of them actuated.

https://doi.org/10.1017/S0263574720000028 Published online by Cambridge University Press

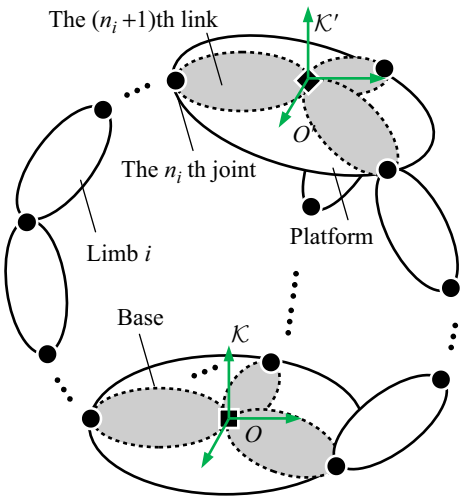

Fig. 1. Schematic diagram of an f-DOF parallel mechanism.

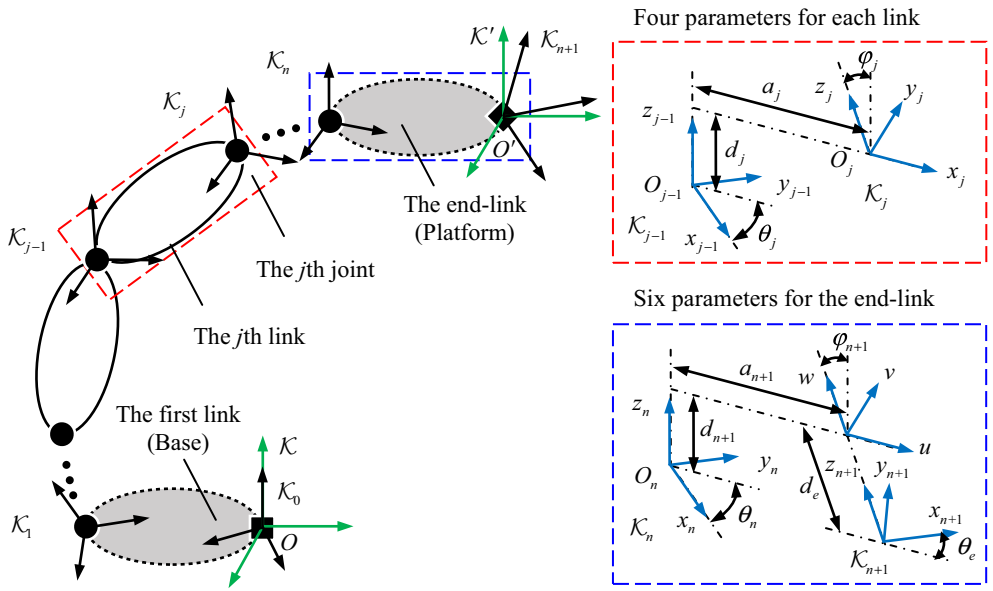

Fig. 2. Definition of coordinate frames in limbs.

Since all limbs share the same platform, the error model of a parallel mechanism can be constructed from the error model of an individual limb. Therefore, we will start from the error model of an arbitrary limb.

2.1. Error model for limbs

In this section, we have n denoted by n_i for convenience. Error modeling of the n-DOF limb uses two global reference frames $\mathcal{K}$ and $\mathcal{K}'$. Here, $\mathcal{K}$ is located at point O on the base, while $\mathcal{K}'$ is located at point O' on the platform and remains parallel to $\mathcal{K}$, as shown in Fig. 2.

The body-fixed frames $\mathcal{K}_0$ and $\mathcal{K}_{n+1}$ are built to describe the geometric errors within the limb, which can also be related to the pose accuracy of the end-link as the frames are attached to the base and platform, respectively, and their origins are coincident with those of $\mathcal{K}$ and $\mathcal{K}'$. Body-fixed frame $\mathcal{K}_j$ is attached to the jth $(j = 1, 2, \cdots, n)$ 1-DOF joint axis with O_j being the origin, the z_j-axis being the joint axis. Two consecutive frames $\mathcal{K}_{j-1}$ and $\mathcal{K}_j$ are defined to satisfy the requirements of the D–H method (Fig. 2). Thus, transforming $\mathcal{K}_{j-1}$ into $\mathcal{K}_j$ requires four steps in the nominal configuration: (1) rotate about the z_{j-1}-axis by θ_j, (2) translate along the z_{j-1}-axis by d_j, (3) translate

https://doi.org/10.1017/S0263574720000028 Published online by Cambridge University Press

along the x_j-axis by a_j, and (4) rotate about the x_j-axis by φ_j. It should be noted that $\mathcal{K}_{n+1}$ can be arbitrarily placed on the platform and $\mathcal{K}_n$ requires another two steps for transformation to $\mathcal{K}_{n+1}$: (5) translate along the z_{n+1}-axis by d_e and (6) rotate about the z_{n+1}-axis by θ_e. Here, subscript e is associated with the end-link.

Let Δ_j denote the pose error produced by the geometric errors of the jth link. Ignoring higher-order terms in the errors, Δ_j evaluated in $\mathcal{K}_j$ can be expressed by

$$\Delta_j = \sum_{m=1}^{4} \eta_{m,j} \hat{\$}_{m,j},\ j = 1, 2, \cdots, n \tag{1}$$

where $\eta_{m,j}$ and $\hat{\$}_{m,j}$ are unexpected small deviation of the mth ($m = 1, 2, \cdots, M$) transformation and the unit twist of that transformation, respectively. The detailed expressions of $\hat{\$}_{m,j}$ are listed in Appendix.

Due to the particularity of the end-link, that is, the $(n+1)$th link, its pose error evaluated in $\mathcal{K}_{n+1}$ can be expressed by

$$\Delta_{n+1} = \sum_{m=1}^{6} \eta_{m,n+1} \hat{\$}_{m,n+1} \tag{2}$$

The detailed expressions of $\hat{\$}_{m,n+1}$ are listed in Appendix.

Evaluated in global reference frame $\mathcal{K}'$, the pose error of the limb, $\$_t$, can be represented as a linear combination of Eqs. (1) and (2) of all links:

$$\$_t = \sum_{j=1}^{n+1} \boldsymbol{A}_j \Delta_j = \sum_{j=1}^{n+1} \boldsymbol{A}_j \boldsymbol{C}_j \boldsymbol{\eta}_j \tag{3}$$

$$\boldsymbol{A}_j = \begin{bmatrix} \boldsymbol{R}_j & \left[\boldsymbol{r}_j \times\right] \boldsymbol{R}_j \\ \boldsymbol{0} & \boldsymbol{R}_j \end{bmatrix},\ \boldsymbol{C}_j = \begin{bmatrix} \hat{\$}_{1,j} \cdots \hat{\$}_{M,j} \end{bmatrix},\ \boldsymbol{\eta}_j = \begin{pmatrix} \eta_{1,j} \\ \vdots \\ \eta_{M,j} \end{pmatrix},\ M = \begin{cases} 4 & j = 1, 2, \cdots, n \\ 6 & j = n+1 \end{cases}$$

where $\boldsymbol{A}_j$ is the adjoint transformation matrix, $\boldsymbol{R}_j$ is the orientation matrix of $\mathcal{K}_j$ with respect to $\mathcal{K}'$, and $\left[\boldsymbol{r}_j \times\right]$ is the skew matrix of vector $\boldsymbol{r}_j$ pointing from O' to O_j. Besides, $\boldsymbol{\eta}_j$ is consisted of structure errors and the $(j-1)$th joint motion error, except for $\boldsymbol{\eta}_1$, which is entirely composed of structure errors of the base.

To reveal which errors can be compensated by regulating the inputs of actuated joints, Eq. (3) can be rewritten as two terms such that the joint motion errors are separated from the structure errors:

$$\$_t = \boldsymbol{T}_a \xi + \boldsymbol{T}_c \boldsymbol{\eta}$$

$$\boldsymbol{T}_a = \begin{bmatrix} \hat{\$}_{ta,2} & \cdots & \hat{\$}_{ta,n+1} \end{bmatrix},\ \boldsymbol{\xi} = \begin{pmatrix} \xi_2 \\ \vdots \\ \xi_{n+1} \end{pmatrix},\ \xi_j = (1-t)\,\eta_{1,j} + t\,\eta_{2,j},\ t = \begin{cases} 0 & R \text{ joint} \\ 1 & \text{P joint} \end{cases}$$

$$\boldsymbol{T}_c = \begin{bmatrix} \boldsymbol{A}_1 \boldsymbol{C}_1 \ \ldots \ \boldsymbol{A}_{n+1} \boldsymbol{C}_{n+1} \end{bmatrix},\ \boldsymbol{\eta} = \begin{pmatrix} \boldsymbol{\eta}_1 \\ \vdots \\ \boldsymbol{\eta}_{n+1} \end{pmatrix} \tag{4}$$

$$\boldsymbol{\eta}_1 = \begin{pmatrix} \eta_{1,1} \\ \vdots \\ \eta_{M,1} \end{pmatrix},\ \boldsymbol{\eta}_j = \begin{pmatrix} t\,\eta_{1,j} \\ (1-t)\,\eta_{2,j} \\ \vdots \\ \eta_{M,j} \end{pmatrix},\ M = \begin{cases} 4 & j = 1, 2, \cdots, n \\ 6 & j = n+1 \end{cases}$$

https://doi.org/10.1017/S0263574720000028 Published online by Cambridge University Press

where ξ_j and $\hat{\$}_{ta,j}$ $(j \neq 1)$ are joint motion errors along/about the $(j-1)$th joint axis and the unit twist of that axis. Here, subscripts a and c are associated with the joint motion errors and structure errors, respectively.

2.2. Error model for parallel mechanism

Noting that all limbs in the parallel mechanism share the same platform (Fig. 1), the pose error twist of the parallel mechanism can then be represented as:[19]

$$\$_t = \$_{t,i} = \boldsymbol{T}_{a,i}\boldsymbol{\xi}_i + \boldsymbol{T}_{c,i}\boldsymbol{\eta}_i,\ i = 1, 2, \cdots, l \tag{5}$$

where subscript i denotes the ith limb.

To solve the pose error twist $\$_t$ from the simultaneousness in Eq. (5), the entire set of applied wrenches exerted on the platform is taken into consideration.[19]

$$\begin{aligned}
\boldsymbol{W} &= [\boldsymbol{W}_a \quad \boldsymbol{W}_c] \\
\boldsymbol{W}_a &= \left[\boldsymbol{W}_{a,1} \ \cdots \ \boldsymbol{W}_{a,f}\right] = \left[\hat{\$}_{wa,g_1,1} \ \cdots \ \hat{\$}_{wa,g_f,f}\right] \\
\boldsymbol{W}_c &= \left[\boldsymbol{W}_{c,1} \ \cdots \ \boldsymbol{W}_{c,l}\right],\ \boldsymbol{W}_{c,i} = \left[\hat{\$}_{wc,1,i} \ \cdots \ \hat{\$}_{wc,6-n_i,i}\right]
\end{aligned} \tag{6}$$

where $\boldsymbol{W}$ is composed by the basic elements of a six-dimensional vector space, which is spanned by the entire set of applied wrenches exerted on the platform; $\hat{\$}_{wa,g_k,k}$ is the unit wrench of actuations associated with the actuated joint, numbered g_k, in the kth $(k = 1, 2, \cdots, f)$ limb; and $\hat{\$}_{wc,g_i,i}$ is the g_ith $(g_i = 1, 2, \cdots, 6-n_i)$ unit wrench of constraints in the ith $(i = 1, 2, \cdots, l)$ limb. Here, subscripts a and c apply to the actuations and constraints, respectively.

In the light of the properties of dual vector space developed in ref. [18], taking inner products on both sides of Eq. (4) with each of $\hat{\$}_{wa,g_a,k}$ and $\hat{\$}_{wc,g_i,i}$ leads to

$$\boldsymbol{W}_a^{\mathrm{T}}\$_t = \boldsymbol{\Lambda}_a\boldsymbol{\xi}_a + \boldsymbol{G}_a\boldsymbol{\eta}_a \tag{7}$$

$$\boldsymbol{W}_c^{\mathrm{T}}\$_t = \boldsymbol{G}_c\boldsymbol{\eta}_c \tag{8}$$

$$\boldsymbol{\Lambda}_a = \mathrm{diag}\left[\hat{\$}_{wa,g_k,k}^{\mathrm{T}}\hat{\$}_{ta,g_k,k}\right],\ \boldsymbol{G}_a = \mathrm{diag}\left[\boldsymbol{W}_{a,k}^{\mathrm{T}}\boldsymbol{A}_k\right],\ \boldsymbol{G}_c = \mathrm{diag}\left[\boldsymbol{W}_{c,i}^{\mathrm{T}}\boldsymbol{A}_i\right]$$

$$\boldsymbol{\xi}_a = \begin{pmatrix} \boldsymbol{\xi}_{g_1,1} \\ \vdots \\ \boldsymbol{\xi}_{g_f,f} \end{pmatrix},\ \boldsymbol{\eta}_a = \begin{pmatrix} \boldsymbol{\eta}_1 \\ \vdots \\ \boldsymbol{\eta}_f \end{pmatrix},\ \boldsymbol{\eta}_c = \begin{pmatrix} \boldsymbol{\eta}_1 \\ \vdots \\ \boldsymbol{\eta}_l \end{pmatrix}$$

Analyses of Eqs. (7) and (8) lead to the following conclusions: related to deviations of actuated joints $\boldsymbol{\xi}_a$, $\boldsymbol{W}_a^{\mathrm{T}}\$_t$ is compensatable by adjusting $\boldsymbol{\xi}_a$ through kinematic calibration; however, the pose error twist $\boldsymbol{W}_c^{\mathrm{T}}\$_t$ is not compensatable and $\boldsymbol{\eta}_c$ should therefore be strictly controlled during the design process and minimized in the processes of manufacture and assembly.

3. Accuracy Design with Reliability Theory

In this section, a commonly used method for tolerance allocation of lower-mobility parallel mechanisms is proposed that involves the use of reliability theory.

3.1. Reliability model for tolerance allocation

For evaluating the geometric accuracy of the mechanism, an accuracy index, $\Delta\lambda$, should be selected according to the use, or structural characteristics, of the mechanism which will be used as the design index at tolerance allocation stage. Without considering the compensatable geometric errors in $\boldsymbol{\eta}_a$, any accuracy design index $\Delta\lambda$ can be expressed as a function of the uncompensatable geometric error vector $\boldsymbol{\eta}_c$.

$$\Delta\lambda = f(\boldsymbol{\eta}_c) \tag{9}$$

where $\boldsymbol{\eta}_c = \left(\eta_{c,1}\ \eta_{c,2} \cdots \eta_{c,n_c}\right)^{\mathrm{T}}$, and n_c is the number of uncompensatable geometric errors.

https://doi.org/10.1017/S0263574720000028 Published online by Cambridge University Press

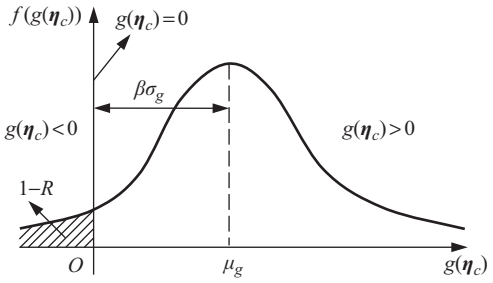

Fig. 3. Physical significance of reliability index β.

The tolerance allocation result of the mechanism is considered acceptable, if index $\Delta\lambda$ is less than a critical limit $\Delta\lambda^*$ (accuracy design requirement). Inspired by this idea, a function of $\Delta\lambda$ can be defined as

$$g(\boldsymbol{\eta}_c) = \Delta\lambda^* - \Delta\lambda = \Delta\lambda^* - f(\boldsymbol{\eta}_c) \tag{10}$$

where $\Delta\lambda^*$ is the largest $\Delta\lambda$ allowed, $g(\boldsymbol{\eta}_c)$ is the performance function where $\eta_{c,i}$ $(i = 1, 2, \cdots, n_c)$ are random variables. When $g(\boldsymbol{\eta}_c) < 0$, the design is in a failure state, and the design index $\Delta\lambda^*$ is not satisfied, whereas when $g(\boldsymbol{\eta}_c) > 0$, it is in a survival state: the limit state is $g(\boldsymbol{\eta}_c) = 0$ which represents a surface in n-dimensional vector space.

In this notation, the accuracy, and its reliability, of the mechanism can be stated as follows:

$$R = P\left\{g(\boldsymbol{\eta}_c) > 0\right\} \tag{11}$$

where $P\{\bullet\}$ denotes the probability that event "$\bullet$" occurs.

Let μ_g and σ_g denote the mean and standard deviation of $g(\boldsymbol{\eta}_c)$. The reliability index can be defined as[26]

$$\beta = \frac{\mu_g}{\sigma_g} \tag{12}$$

If $\Phi(\bullet)$ represents the cumulative distribution of the standard normal variable, we have[26]

$$R = \Phi(\beta) \tag{13}$$

As shown in Fig. 3, β is proportional to μ_g and inversely proportional to σ_g: the higher the value of β, the higher the reliability R. According to Eqs. (10)–(13), it can be seen that, once R or β is given, one constraint equation with respect to $\eta_{c,i}$ can be established, which will be useful in the following tolerance allocation process.

3.2. Tolerance allocation with FOSM algorithm

In probability theory, the random moments of a function with random input variables can be determined by a probabilistic, first-order second-moment (FOSM) method. Here, "first-order" means that when calculated, only the first-order term of the Taylor expansion is retained; moreover, "second-moment" indicates that FOSM is used to calculate the variance of a target variable ($g(\boldsymbol{\eta}_c)$), which can quantify the uncertainty in a problem.

Since the elements in $\boldsymbol{\eta}_c$ are mutually independent, the performance function $g(\boldsymbol{\eta}_c)$ can be approximated by $\tilde{g}(\boldsymbol{\eta}_c)$:

$$\tilde{g}(\boldsymbol{\eta}_c) = g(\boldsymbol{\mu}) + \nabla g(\boldsymbol{\mu})^{\mathrm{T}}\left(\boldsymbol{\eta}_c - \boldsymbol{\mu}\right) \tag{14}$$

$$\boldsymbol{\mu} = \left(\boldsymbol{\mu}_1\ \mu_2 \cdots \mu_{n_c}\right)^{\mathrm{T}},\ \nabla g\ (\mu) = \left[\frac{\partial g(\boldsymbol{\mu})}{\partial \mu_1}\ \frac{\partial g(\boldsymbol{\mu})}{\partial \mu_2} \cdots \frac{\partial g(\boldsymbol{\mu})}{\partial \mu_{n_c}}\right]^{\mathrm{T}}$$

where $\boldsymbol{\mu}$ is the mean vector of $\boldsymbol{\eta}_c$, $\frac{\partial g(\boldsymbol{\mu})}{\partial \mu_i}$ is the partial derivative of $g(\boldsymbol{\eta}_c)$ at the mean vector $\boldsymbol{\mu}$ with respect to the ith entry of $\boldsymbol{\eta}_c$, and $\nabla g(\boldsymbol{\mu})$ is the gradient vector of $g(\boldsymbol{\eta}_c)$ at $\boldsymbol{\mu}$. The mean and variance of $\tilde{g}(\boldsymbol{\eta}_c)$ can thus be determined

https://doi.org/10.1017/S0263574720000028 Published online by Cambridge University Press

$$\mu_{\tilde{g}} \approx E\left[g(\boldsymbol{\mu})\right] = g(\boldsymbol{\mu}) \tag{15}$$

$$\sigma_{\tilde{g}}^2 = V\left[\tilde{g}(\boldsymbol{\mu})\right] = V\left[g(\boldsymbol{\mu})\right] + \left[\nabla g(\boldsymbol{\mu})^{\mathrm{T}}\right]^2 V\left[\boldsymbol{\eta}_c\right] \tag{16}$$

where

$$V\left[\boldsymbol{\eta}_c\right] = \left[\, V\left[\eta_{c,1}\right]\, V\left[\eta_{c,2}\right] \cdots V\left[\eta_{c,n_c}\right]\right]^{\mathrm{T}}$$

The reliability index can then be redefined as

$$\beta = \mu_{\tilde{g}} / \sigma_{\tilde{g}} \tag{17}$$

which directly describes the relationship between reliability index and the mean and variance of the design variable $\boldsymbol{\eta}_c$. In summary, according to the Taylor expansion of the performance function $g\,(\eta_c)$, Eqs. (15) and (16) can be used to reveal the key algorithms of the FOSM probabilistic method and will be used in the following tolerance allocation process.

According to Eq. (16), the sensitivity of $\Delta\lambda$ with respect to $\eta_{c,i}$, representing the standard deviation of $\Delta\lambda$ caused by the unit standard deviation of $\eta_{c,i}$, can be defined as

$$\omega_i = \left| \frac{\partial g(\boldsymbol{\eta}_c)}{\partial \eta_{c,i}} \right|, i = 1, 2, \cdots, n \tag{18}$$

Assuming that all the geometric errors in $\boldsymbol{\eta}_c$ have the same effect on $\Delta\lambda$, we have

$$\omega_1^2 V\left[\eta_{c,1}\right] = \omega_2^2 V\left[\eta_{c,2}\right] = \cdots = \omega_n^2 V\left[\eta_{c,n_c}\right] \tag{19}$$

Combining Eqs. (15) to (19), the relationship between $\sigma[\eta_{c,i}]$ and β can be obtained:

$$\sigma[\eta_{c,i}] = \frac{1}{\sqrt{n}} \frac{\Delta\lambda^*}{\omega_i} \frac{1}{\beta}, i = 1, 2, \cdots, n_c \tag{20}$$

Thus, given the reliability index β or the tolerance allocation reliability R, the allocated tolerance of each geometric error, $\pm\sigma[\eta_{c,i}]$, can be obtained.

4. An Example

Here, the proposed method is applied to a machining hybrid robot[27] which is formed of a 3-DOF positioning parallel mechanism and a 2-DOF wrist (Fig. 4). Simulations are used to verify the effectiveness of the tolerance allocation method.

4.1. Brief description of the mechanism

The hybrid robot under investigation is used for aeronautical component manufacturing (Fig. 4): its basic structure is the over-constrained R(2-R$\underline{\text{P}}$S&RP)&U$\underline{\text{P}}$S parallel mechanism. Herein, we use P, R, U, and S to denote prismatic, revolute, universal, and spherical joints, respectively, and the underlined $\underline{\text{P}}$ represents an actuated prismatic joint. It comprises a 6-DOF U$\underline{\text{P}}$S spatial limb plus a stand-alone 1T1R planar parallel mechanism, and at each side of the base link, there is a pair of R joints connecting the properly constrained non-actuated RP limb to the machine frame. The base is located at the rearmost R joints of the two actuated R$\underline{\text{P}}$S limbs and the R and P joints of the RP limb forming a three-in-one part, which is a key feature of the robot. In this section, we will focus on error modeling and tolerance allocation of the parallel mechanism, since it forms the main body of the hybrid robot.

4.2. Error modeling

According to the proposed modeling method (Section 2), the coordinate system of the R(2-R$\underline{\text{P}}$S&RP)&U$\underline{\text{P}}$S parallel mechanism is established (Fig. 5). The transformation parameters of adjacent frames in four limbs are listed in Tables I and II.

For this particular problem, considering the bases of the wrench sub-spaces of each limb, we have $\hat{\$}_{wa,g_a,k}$ in $\boldsymbol{W}_a$ and $\hat{\$}_{wc,g_i,i}$ in $\boldsymbol{W}_c$ expressed as:

https://doi.org/10.1017/S0263574720000028 Published online by Cambridge University Press

Table I. D–H parameters of the ith ($i = 1, 2, 3$) limb.

Link j	**$\theta_{j,i}$(rad)**	**$d_{j,i}$(mm)**	**$a_{j,i}$(mm)**	**$\varphi_{j,i}$(rad)**	**d_e(mm)**	**θ_e(rad)**
1	0	0	αb_i	$\pi/2$		
2	$\xi_{1,i}+\pi/2$	$(1-\alpha)\, b_i$	0	$\pi/2$		
3	$\xi_{2,i}+\pi/2$	0	0	$\pi/2$		
4	0	$\xi_{3,i}$	0	0		
5	$\xi_{4,i}+(1-\alpha)\,\pi/2$	0	0	$\pi/2$		
6	$\xi_{5,i}+\pi/2$	0	0	$\pi/2$		
7	$\xi_{6,i}+\pi/2$	0	e_i	$\pi/2$	0	$\pi/2+\pi\alpha/2$

Note: (1) if $i = 1$, $\alpha = 1$, else $\alpha = 0$;
(2) $\xi_{j,i}$ denotes the motion of the jth joint in the ith limb;
(3) b_i and e_i denote structure parameters of the base and end-link.

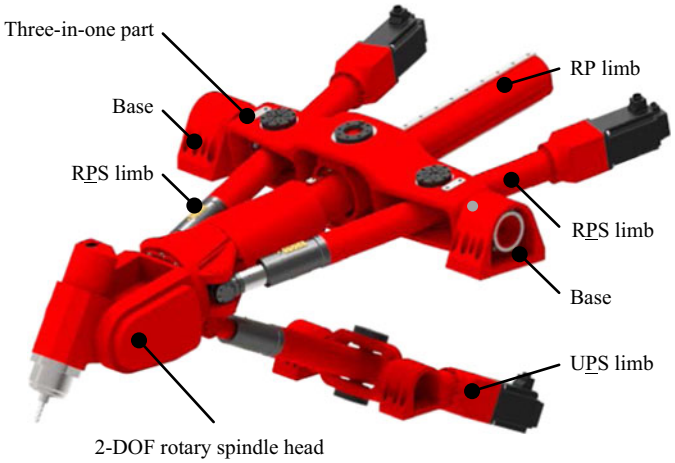

Fig. 4. 3D CAD model of the 5-DOF hybrid robot.

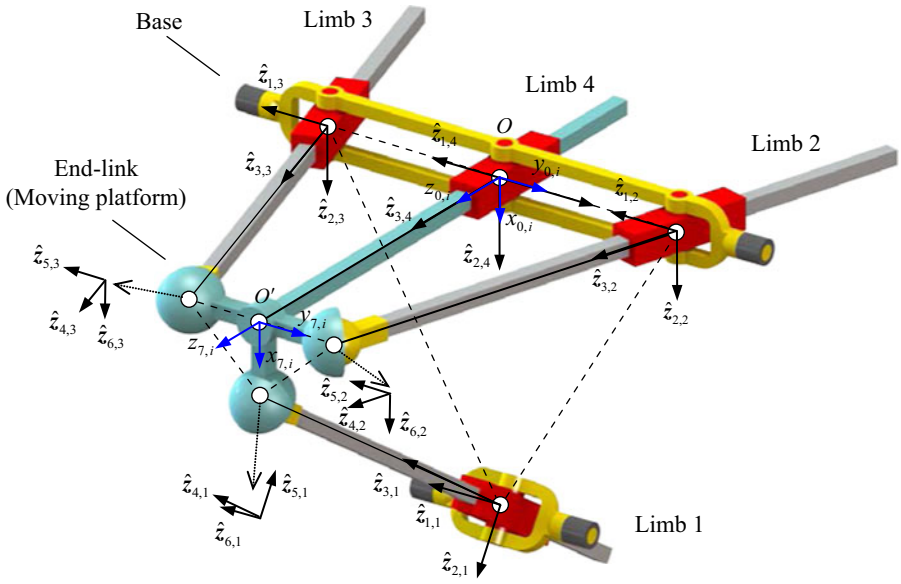

Fig. 5. Configuration and coordinate frames of the R(2-RPS&RP)&UPS parallel mechanism.

https://doi.org/10.1017/S0263574720000028 Published online by Cambridge University Press

Table II. D–H parameters of the ith ($i = 4$) limb (the UP limb).

Link j	$\theta_{j,i}$**(rad)**	$d_{j,i}$**(mm)**	$a_{j,i}$**(mm)**	$\varphi_{j,i}$**(rad)**	d_e**(mm)**	θ_e**(rad)**
1	0	0	0	$\pi/2$		
2	$\xi_{1,i}+\pi/2$	0	0	$\pi/2$		
3	$\xi_{2,i}+\pi/2$	0	0	$\pi/2$		
4	0	$\xi_{3,i}$	0	0	0	$\pi/2$

$$\hat{\$}_{wa,3,k} = \begin{pmatrix} \hat{z}_{3,k} \\ \boldsymbol{a}_i \times \hat{z}_{3,k} \end{pmatrix}, k = 1,2,3$$

$$\hat{\$}_{wc,1,4} = \begin{pmatrix} \mathbf{0} \\ \boldsymbol{n}_{1,4} \end{pmatrix}, \hat{\$}_{wc,2,4} = \begin{pmatrix} \hat{z}_{2,4} \\ -\boldsymbol{\xi}_{3,4}\hat{z}_{3,4} \times \hat{z}_{2,4} \end{pmatrix}, \hat{\$}_{wc,3,4} = \begin{pmatrix} \boldsymbol{n}_{2,4} \\ -\boldsymbol{\xi}_{3,4}\hat{z}_{3,4} \times \boldsymbol{n}_{2,4} \end{pmatrix}$$

$$\boldsymbol{n}_{1,4} = \hat{z}_{1,4} \times \hat{z}_{2,4}, \boldsymbol{n}_{2,4} = \hat{z}_{1,4} \times \hat{z}_{3,4}$$

The geometric error model can then be written as

$$\boldsymbol{W}_a^{\mathrm{T}}\$_t = \boldsymbol{\Lambda}_a\boldsymbol{\xi}_a + \boldsymbol{G}_a\boldsymbol{\eta}_a \tag{21}$$

$$\boldsymbol{W}_c^{\mathrm{T}}\$_t = \boldsymbol{G}_c\boldsymbol{\eta}_c \tag{22}$$

Taking advantage of symbolic and numerical solvers, explicit expressions for $\boldsymbol{G}_a$, $\boldsymbol{\eta}_a$ in Eq. (21) and $\boldsymbol{G}_c$, $\boldsymbol{\eta}_c$ in Eq. (22) can be derived as

$$\boldsymbol{G}_a = \mathrm{diag}\left[\boldsymbol{G}_{a,k}\right], \boldsymbol{\eta}_a = \left(\boldsymbol{\eta}_{a,1}^{\mathrm{T}}\ \boldsymbol{\eta}_{a,2}^{\mathrm{T}}\ \boldsymbol{\eta}_{a,3}^{\mathrm{T}}\right)^{\mathrm{T}}$$

$$\boldsymbol{G}_{a,i} = \left(-b_i \mathrm{s}\xi_{2,\mathrm{i}}\ c\xi_{1,i}c\xi_{2,i}\ -c\xi_{2,i}s\xi_{1,i}\ s\xi_{2,i}\ c\xi_{2,i}\ 1\ c\xi_{5,i}\ s\xi_{5,i}\ -c\xi_{5,i}s\xi_{6,i}\ c\xi_{5,i}c\xi_{6,i}\ -a_i\mathrm{s}\xi_{5,i}\right), i = 1$$

$$\boldsymbol{\eta}_{a,i} = \left(\delta\theta_{1,i}\ \delta d_{1,i}\ \delta a_{1,i}\ \delta d_{2,i}\ \delta a_{2,i}\ \delta d_{5,i}\ \delta a_{6,i}\ \delta d_{7,i}\ \delta a_{7,i}\ \delta d_{e,i}\ \delta\theta_{e,i}\right)^{\mathrm{T}}, i = 1$$

$$\begin{aligned}\boldsymbol{G}_{a,i} = \big(&-b_i \mathrm{s}\xi_{1,i}\mathrm{c}\xi_{2,i}\ c\xi_{1,i}c\xi_{2,i}\ -s\xi_{1,i}c\xi_{2,i}\ -b_i\mathrm{c}\xi_{1,i}\mathrm{c}\xi_{2,i}\ s\xi_{2,i}\ c\xi_{2,i}\ 1\ c\xi_{5,i}\ \mathrm{s}\xi_{5,i}\\ &-c\xi_{5,i}s\xi_{6,i}\ c\xi_{5,i}c\xi_{6,i}\ -a_i\mathrm{s}\xi_{5,1}\big), i = 2,3\end{aligned}$$

$$\boldsymbol{\eta}_{a,i} = \left(\delta\theta_{1,i}\ \delta d_{1,i}\ \delta a_{1,i}\ \delta\varphi_{1,i}\ \delta d_{2,i}\ \delta a_{2,i}\ \delta d_{5,i}\ \delta a_{6,i}\ \delta d_{7,i}\ \delta a_{7,i}\ \delta d_{e,i}\ \delta\theta_{e,i}\right)^{\mathrm{T}}, i = 2,3$$

$$\boldsymbol{G}_c = \left[\boldsymbol{G}_{c1}^{\mathrm{T}}\ \boldsymbol{G}_{c2}^{\mathrm{T}}\ \boldsymbol{G}_{c3}^{\mathrm{T}}\right]^{\mathrm{T}}$$

$$\boldsymbol{G}_{c1} = \left(\mathrm{c}\xi_{1,4}\,0\,0\ -\mathrm{s}\xi_{1,4}\,0\,0\,1\,0\,0\ -\mathrm{s}\xi_{2,4}\,\mathrm{c}\xi_{2,4}\,0\ -\mathrm{s}\xi_{2,4}\,\mathrm{c}\xi_{2,4}\right)$$

$$\boldsymbol{G}_{c2} = \left(0\ s\xi_{1,4}\ c\xi_{1,4}\,0\,0\,0\,0\,1\,0\,0\ \ 0\,0\,\xi_{3,4}\,0\right)$$

$$\boldsymbol{G}_{c3} = \left(0\ -c\xi_{1,4}\ s\xi_{2,4}\ s\xi_{1,4}\ s\xi_{2,4}\,0\,c\xi_{2,4}\ \ -s\xi_{2,4}\ \ 0\,0\,1\,0\,0\,1\,0\,0\right)$$

$$\boldsymbol{\eta}_c = \left(\delta\theta_{1,4}\ \delta d_{1,4}\ \delta a_{1,4}\ \delta\varphi_{1,4}\ \delta d_{2,4}\ \delta a_{2,4}\ \delta\varphi_{2,4}\ \delta d_{3,4}\ \delta a_{3,4}\ \delta\varphi_{3,4}\ \delta\theta_{4,4}\ \delta a_{4,4}\ \delta\varphi_{4,4}\ \delta\theta_{e,4}\right)^{\mathrm{T}}$$

Here, "s·" and "c·" denote "sin(·)" and "cos(·)", and subscript e refers to the error element of the end-link.

As proved elsewhere,[19] one geometric error is uncompensatable, if, and only if, it meets the following two conditions simultaneously: (1) it is an error of an under-constrained or properly constrained limb and (2) its projection on the twist sub-space of restrictions is non-zero. For the lower-mobility parallel mechanism under investigation, limbs 1, 2, and 3 are non-constrained limbs, and limb 4 is a properly constrained non-actuated limb. Therefore, only the geometric errors in limb 4 are uncompensatable.

https://doi.org/10.1017/S0263574720000028 Published online by Cambridge University Press

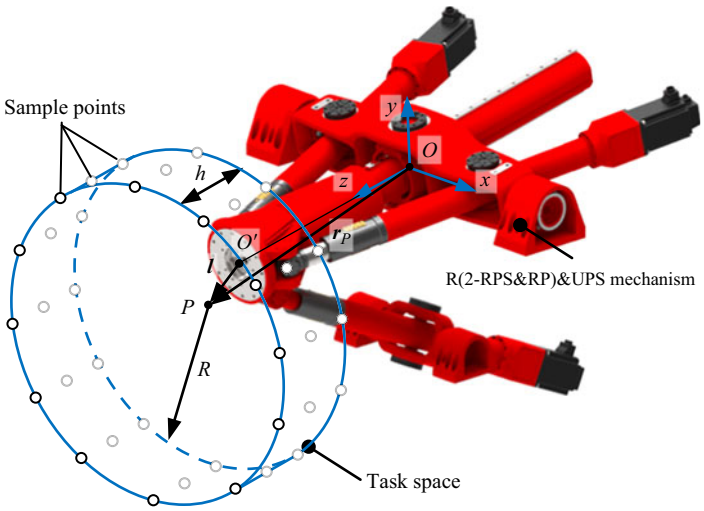

Fig. 6. The task space of the R(2-RPS&RP)&UPS mechanism within the 5-DOF hybrid robot.

4.3. Error analysis and tolerance allocation

Considering the detailed nature of the structure of this mechanism, the intersection P of the two mutually vertical axes of the 2-DOF rotary head is selected as the reference point, and its volumetric error is defined as the accuracy design index:

$$\Delta\lambda = \|\Delta \boldsymbol{r} + \Delta\boldsymbol{\theta} \times \boldsymbol{l}\| \tag{23}$$

where $\Delta\boldsymbol{r}$ and $\Delta\boldsymbol{\theta}$ are position and orientation error vectors of the moving platform which arose from $\boldsymbol{\eta}_c$ alone, and $\boldsymbol{l}$ is the position vector from O' to P. Since $\Delta\lambda$ covers both positional and orientational information of the parallel mechanism, $\Delta\lambda$ is reasonable and effective for tolerance design purposes.

Theoretically, the relationship between $\Delta\lambda$ and $\boldsymbol{\eta}_c$ changes with the movement of the mechanism: in other words, $\Delta\lambda$ is a function that depends on $\boldsymbol{\eta}_c$ and $\boldsymbol{r}_P$, the position vector of P measured in frame O (Fig. 6).

$$\Delta\lambda = f(\boldsymbol{r}_P, \boldsymbol{\eta}_c) \tag{24}$$

To ensure the validity of the tolerance allocation method throughout the task space, one special $\boldsymbol{r}_P$ should be determined to make $\Delta\lambda$ most sensitive to $\boldsymbol{\eta}_c$. For this purpose, MCS, which is a method used to solve complex problems using random numbers and probability, is adopted by following these steps:

Step 1: Select $m = 147$ evenly spaced sample points $\boldsymbol{r}_{P,j}$ $(j = 1, 2, \cdots, m)$ in the whole task space (Fig. 6);
Step 2: Assume that every geometric error in $\boldsymbol{\eta}_c$ obeys the standard normal distribution, $\eta_{c,i} \sim N(0, 1)$, and generate random value of $\eta_{c,i}$ based on its probability distribution $(i = 1, 2, \cdots, n_c)$;
Step 3: Substitute $\eta_{c,i}$ and $\boldsymbol{r}_{P,j}$ into the function $\Delta\lambda = f(\boldsymbol{r}_P, \boldsymbol{\eta}_c)$ to obtain a set of random $\Delta\lambda_j$ $(j = 1, 2, \cdots, m)$;
Step 4: With the calculation repeated 10^4 times, estimate the standard deviation of $\Delta\lambda_j$, $\sigma[\Delta\lambda_j]$;
Step 5: Find the largest $\sigma[\Delta\lambda_j]$, and the corresponding $\boldsymbol{r}_{P,j}$ is the desired position.

The simulation resulting from the aforementioned process is shown in Fig. 7, where the radius of each error sphere denotes the standard deviation of $\Delta\lambda_j$ at the jth sample point. It can be found that $\sigma[\Delta\lambda_j]$ is more sensitive to changes in the x-coordinate. The position with the largest standard deviation of $\Delta\lambda_j$ is $\boldsymbol{r}_{P,32} = \begin{pmatrix} -600 & 0 & 1000 \end{pmatrix}^{\mathrm{T}}$ mm and $\sigma[\Delta\lambda_{32}] = 0.96\,\mu$m. In the view of probability, $\boldsymbol{r}_{P,32}$ has the highest possibility of being the position of maximum volumetric error over the whole task space. Therefore, it is reasonable to choose $\boldsymbol{r}_{P,32}$ for the following sensitivity analysis and tolerance allocation.

https://doi.org/10.1017/S0263574720000028 Published online by Cambridge University Press

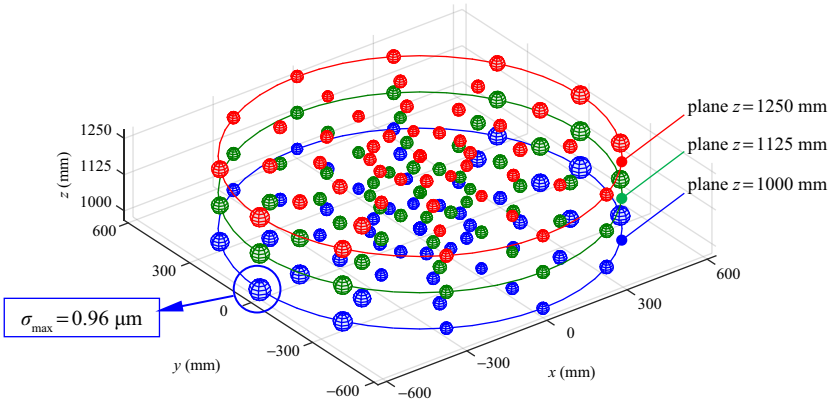

Fig. 7. Error-sensitive point selection with the MCS method.

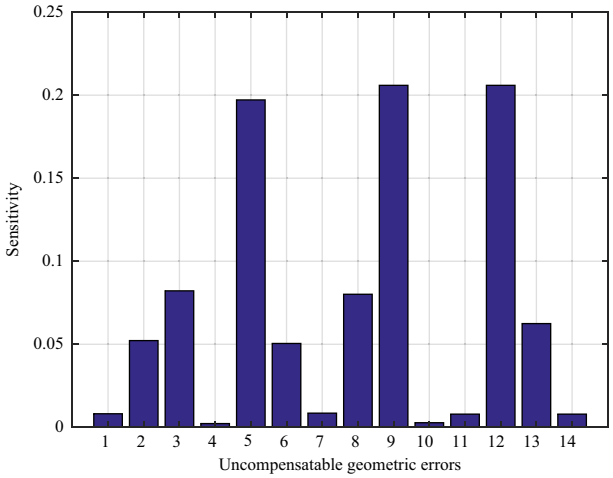

Fig. 8. Sensitivity analysis of uncompensatable geometric errors in $\boldsymbol{\eta}_c$.

The sensitivities of geometric errors in $\boldsymbol{\eta}_c$ given by Eq. (18) are calculated and shown in Fig. 8. It can be seen that $\eta_{c,i}(i = 1, 4, 7, 10, 11, 14)$ has some effect on $\Delta\lambda$, while $\eta_{c,5}(\delta d_{2,4})$, $\eta_{c,9}(\delta a_{3,4})$ and $\eta_{c,12}(\delta a_{4,4})$ exert significant influences on $\Delta\lambda$, which should therefore be restricted in accuracy design.

Since the hybrid robot composed of this R(2-RPS&RP)&UPS parallel mechanism is used for machining and expected to reach the accuracy level of mid-range numerical control machine tools, the design index $\Delta\lambda^*$ is chosen to be 0.05 mm. Given the reliability index β varies from 0.5 to 3.0, the reliability R and the allocated tolerance $\pm\sigma[\eta_{c,i}]$ of each uncompensatable geometric error can be obtained using Eqs. (14) and (20). The tolerance allocation results are listed in Table III. It can be seen that, when $\beta = 2.0$, the reliability R reaches 97.72%, which can meet the reliability requirement for accuracy design of this mechanism. In this case, the tolerances of all uncompensatable geometric errors are determined.

4.4. Verification

Mechanism performance is considered acceptable, if the design index $\Delta\lambda$, the volumetric error of the reference point on the platform, is less than a critical limit $\Delta\lambda^*$. The accuracy reliability R represents the probability that the index $\Delta\lambda$ lies within a specified limit $\Delta\lambda^*$ for all points in the workspace. In consideration of this, MCS is adopted to verify the effectiveness of the tolerance allocation results:

Step 1: Randomly select one point (x_i, y_i, z_i) within the whole task space;
Step 2: Assume that the tolerance τ_i corresponding to the ith error element $\eta_{c,i}$ $(i = 1, 2, \cdots, n_c)$ follows a uniform distribution on the interval $[-\sigma[\eta_{c,i}],\ \sigma[\eta_{c,i}]]$,[28] $\tau_i \sim U[-\sigma[\eta_{c,i}],\ \sigma[\eta_{c,i}]]$ and generate τ_i based on its probability distribution;

https://doi.org/10.1017/S0263574720000028 Published online by Cambridge University Press

Table III. Tolerance allocation results for uncompensatable geometric errors.

Reliability index β		0.5	1.0	1.5	2.0	2.5	3.0
Reliability R (%)		69.14	84.13	93.32	97.72	99.38	99.87
	No.	Allocated tolerance values (unit: mm)					
Allocated tolerances ($\pm\sigma[\eta_{c,i}]$) of all the uncompensatable geometric errors	1	±3.271	±1.635	±1.090	±0.818	±0.654	±0.545
	2	±0.512	±0.256	±0.171	±0.128	±0.102	±0.085
	3	±0.325	±0.163	±0.108	±0.081	±0.065	±0.054
	4	±11.854	±5.927	±3.951	±2.963	±2.371	±1.976
	5	±0.136	±0.068	±0.045	±0.034	±0.027	±0.023
	6	±0.529	±0.265	±0.176	±0.132	±0.106	±0.088
	7	±3.133	±1.566	±1.044	±0.783	±0.627	±0.522
	8	±0.334	±0.167	±0.111	±0.083	±0.067	±0.056
	9	±0.130	±0.065	±0.043	±0.032	±0.026	±0.022
	10	±9.639	±4.819	±3.213	±2.410	±1.928	±1.606
	11	±3.366	±1.683	±1.122	±0.842	±0.673	±0.561
	12	±0.130	±0.065	±0.043	±0.032	±0.026	±0.022
	13	±0.428	±0.214	±0.143	±0.107	±0.086	±0.071
	14	±3.366	±1.683	±1.122	±0.842	±0.673	±0.561

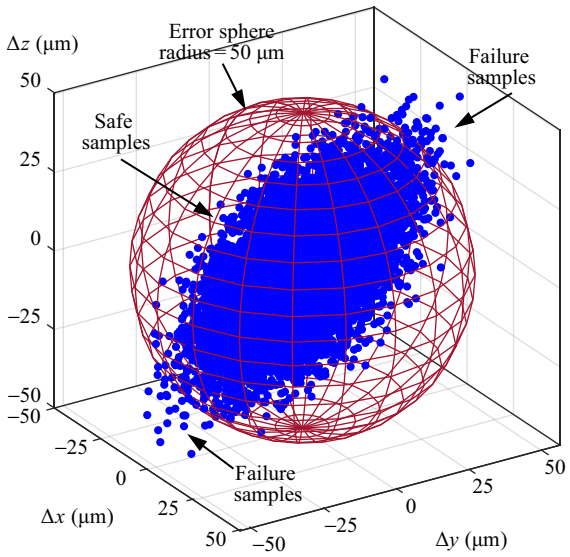

Fig. 9. Illustration of failure/safe samples within the whole task space.

Step 3: Estimate the volumetric error $\Delta\lambda$ using inverse kinematics and the error model;
Step 4: Repeat steps 1 through 3 10^4 times, analyze the statistical characteristics of $\Delta\lambda$, and predict the accuracy reliability R.

In Fig. 9, 10^4 simulated samples of $\Delta\lambda$ are plotted along with a sphere of radius equal to the critical limit of volumetric error, $\Delta\lambda^* = 50$ μm. Thus, all cases of $\Delta\lambda > \Delta\lambda^*$ represent failures of the mechanism which cannot meet the specified pose accuracy. As shown in Fig. 10, the histogram illustrates the distribution of the simulated $\Delta\lambda$ values. Consequently, the mean $\Delta\lambda$ and its standard deviation are 21.97 and 9.42 μm, respectively, and only 1.13% of samples fall into the failure region, so that is to say, the reliability R reaches 98.87% for this tolerance allocation problem, which proves the effectiveness of the proposed approach.

4.5. Comparison with traditional method

In the traditional tolerance allocation method, all geometric errors ($\boldsymbol{\eta}_a$ and $\boldsymbol{\eta}_c$) are analyzed and allocated together. The allocated tolerances are often too tight to be realized in engineering practice,

https://doi.org/10.1017/S0263574720000028 Published online by Cambridge University Press

Table IV. Number of geometric errors.

Number	Geometric errors	Variable	Limb
1, …, 14	$\delta\theta_{1,4},\ \delta d_{1,4},\ \delta a_{1,4},\ \delta\varphi_{1,4},\ \delta d_{2,4},\ \delta a_{2,4},\ \delta\varphi_{2,4},\ \delta d_{3,4},\ \delta a_{3,4},\ \delta\varphi_{3,4},\ \delta\theta_{4,4},\ \delta a_{4,4},\ \delta\varphi_{4,4},\ \delta\theta_{e,4}$	$\boldsymbol{\eta}_c$	4
15, 16, 17	$\xi_{a,1},\ \xi_{a,2},\ \xi_{a,3}$	$\boldsymbol{\xi}_a$	1,2,3
18, …, 28	$\delta\theta_{1,1},\ \delta d_{1,1},\ \delta a_{1,1},\ \delta d_{2,1},\ \delta a_{2,1},\ \delta d_{5,1},\ \delta a_{6,1},\ \delta d_{7,1},\ \delta a_{7,1},\ \delta d_{e,1},\ \delta\theta_{e,1}$	$\boldsymbol{\eta}_{a,1}$	1
29, …, 40	$\delta\theta_{1,2},\ \delta d_{1,2},\ \delta a_{1,2},\ \delta\varphi_{1,2},\ \delta d_{2,2},\ \delta a_{2,2},\ \delta d_{5,2},\ \delta a_{6,2},\ \delta d_{7,2},\ \delta a_{7,2},\ \delta d_{e,2},\ \delta\theta_{e,2}$	$\boldsymbol{\eta}_{a,2}$	2
41, …, 52	$\delta\theta_{1,3},\ \delta d_{1,3},\ \delta a_{1,3},\ \delta\varphi_{1,3},\ \delta d_{2,3},\ \delta a_{2,3},\ \delta d_{5,3},\ \delta a_{6,3},\ \delta d_{7,3},\ \delta a_{7,3},\ \delta d_{e,3},\ \delta\theta_{e,3}$	$\boldsymbol{\eta}_{a,3}$	3

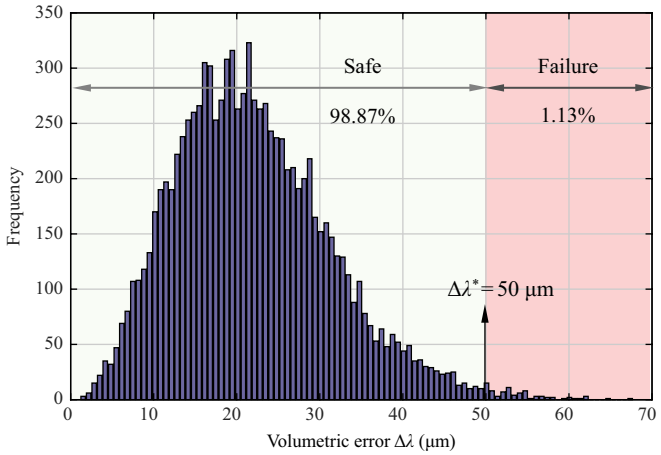

Fig. 10. Frequency distribution histogram of the evaluated volumetric error $\Delta\lambda$.

since too many geometric errors have to be taken into consideration. However, in the light of the new modeling and tolerance allocation method proposed here, all geometric errors can be separated into two groups $\boldsymbol{\eta}_a$ and $\boldsymbol{\eta}_c$. Only uncompensatable error vector $\boldsymbol{\eta}_c$ should be considered in the tolerance allocation process, and this can be minimized in the processes of manufacture and assembly, since the pose error twist $\boldsymbol{W}_a^{\mathrm{T}}\$_t$ aroused by $\boldsymbol{\eta}_a$ can be compensated by adjusting $\boldsymbol{\xi}_a$ with kinematic calibration such that:

$$\boldsymbol{\xi}_a = -\boldsymbol{\Lambda}_a^{-1}\boldsymbol{G}_a\boldsymbol{\eta}_a \tag{25}$$

To compare these two methods, the same analysis and allocation simulations are carried out using traditional method with the same indices $\Delta\lambda^* = 50\,\mu\mathrm{m}$ and $R = 97.72\%$. The tolerance allocation results considering all geometric errors are shown in Fig. 11, and the sequence numbers of geometric errors are listed in Table IV. In Fig. 11, the red area on the left and the green area on the right represent the tolerance allocation results of uncompensatable and compensatable geometric errors obtained by traditional methods, respectively. Due to the great difference of each data, the larger values in the graph are directly represented by numbers above the graph. The geometric errors with the value of +8 have no effect on the accuracy design index, and the tolerance design values can be determined according to the experience or manufacturing capacity. Compared with the results obtained by the new method (as listed in Table 3 under the column containing the value $R = 97.72\%$), it can be seen that (1) on the premise of ensuring that the pose accuracy meets the design requirements with the same reliability, the tolerances obtained by the traditional method are tighter; thus, more manufacturing costs are required to ensure these tolerances; (2) for the traditional method, several geometric errors with extremely strict tolerances, such as $\xi_{a,i}$, $\delta\theta_{1,i}$, and $\delta d_{5,i}$, can hardly be realized in practical manufacturing processes. Therefore, the proposed method is more practical and reasonable than

https://doi.org/10.1017/S0263574720000028 Published online by Cambridge University Press

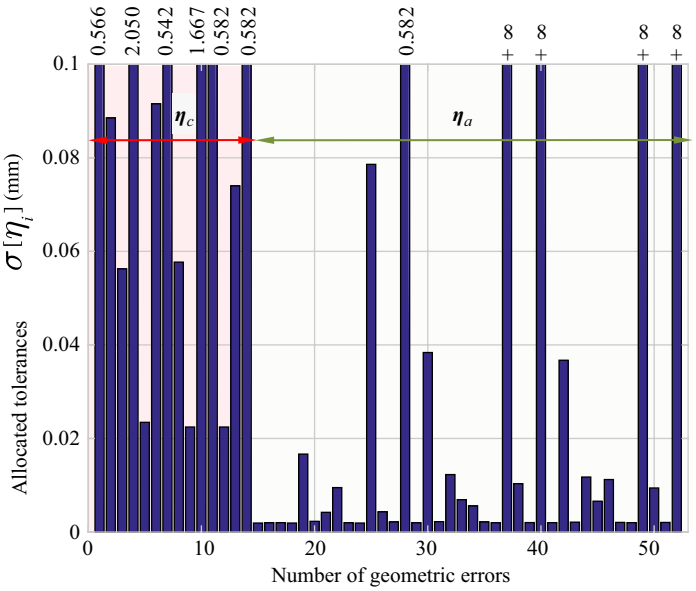

Fig. 11. Tolerance allocation results of all geometric errors using the traditional method.

the traditional one when dealing with the problem of tolerance allocation for robotized machine tools.

5. Conclusions

This paper presents a general method for geometric error modeling and accuracy design of lower-mobility parallel mechanisms. The following conclusions can be drawn:

1. The proposed error modeling approach is general and systematic, and allows the geometric errors affecting the compensatable and uncompensatable pose accuracy of the end-effector to be separated. The geometric errors that affect the uncompensatable pose error of the mechanism should be minimized during the processes of design, manufacture, and assembly.
2. The proposed tolerance allocation approach is efficient and accurate, giving each uncompensatable geometric error an appropriate tolerance based on reliability theory, which can ensure that the pose accuracy satisfies the required index over the whole workspace with any given probability.
3. The proposed methods have been successfully applied to a hybrid machining robot, which is composed of an R(2-RPS&RP)&UPS lower-mobility parallel mechanism, and the effectiveness thereof is verified by MCS.

Acknowledgments

This work is supported by the National Key Research and Development Program (Grant 2017YFE0111300) and the National Natural Science Foundation of China (Grant 51775376).

References

1. L. Uriarte, M. Zatarain, D. Axinte, J. Yagüe-Fabra, S. Ihlenfeldt, J. Eguia and A. Olarra, "Machine tools for large parts," *CIRP Ann.-Manuf. Technol.* **62**(2), 731–750 (2013).
2. N. Hennes and D. Staimer, "Application of PKM in Aerospace Manufacturing-High Performance Machining Centres ECOSPEED, ECOSPEED-F and ECOLINER," *Proceedings of the 4th Chemnitz Parallel Kinematics Seminar*, Chemnitz (2004) pp. 557–577.
3. B. Siciliano, "The Tricept robot: Inverse kinematics, manipulability analysis and closed-loop direct kinematics algorithm," *Robotica* **17**(17), 437–445 (1999).
4. K. E. Neumann, "The Key to Aerospace Automation," *SAE Aerospace Manufacturing and Automated Fastening Conference and Exhibition*, Detroit (2006) pp. 01–3144.
5. M. Weck and D. Staimer, "Parallel kinematic machine tools – current state and future potentials," *CIRP Ann.-Manuf. Technol.* **51**(2), 671–683 (2002).

https://doi.org/10.1017/S0263574720000028 Published online by Cambridge University Press

6. W. Tian, F. Yin, H. Liu, J. Li, Q. Li, T. Huang and D. G. Chetwynd, "Kinematic calibration of a 3-DOF spindle head using a double ball bar," *Mech. Mach. Theory* **102**, 167–178 (2016).
7. Y. Hu, F. Gao, X. Zhao, B. Wei, D. Zhao and Y. Zhao, "Kinematic calibration of a 6-DOF parallel manipulator based on identifiable parameters separation (IPS)," *Mech. Mach. Theory* **126**, 61–78 (2018).
8. P. Schellekens, N. Rosielle, H. Vermeulen, M. Vermeulen, S. Wetzels and W. Pril, "Design for precision: current status and trends," *CIRP Ann.-Manuf. Technol.* **47**(2), 557–586 (1998).
9. J. Liu and Y. Zhang, "Improving the positioning accuracy of a neurosurgical robot system," *IEEE/ASME T. Mech.* **12**(5), 527–533 (2007).
10. C. D. Wang, X. J. Wang, X. D. Chen and C. H. Zhang, "Error analysis of 6-DOF welding robot," *Appl. Mech. Mater.* **220–223**, 1111–1115 (2012).
11. S. L. Cai, L. B. Peng and W. T. Huang, "Error analysis of a 2-PRS/2-UPS 4-DOF parallel platform," *Adv. Mater. Res.* **605–607**, 1511–1514 (2013).
12. P. Huang, J. Wang, L. Wang and R. Yao, "Identification of structure errors of 3-PRS-XY mechanism with regularization method," *Mech. Mach. Theory* **46**(7), 927–944 (2011).
13. I. M. Chen, G. Yang, C. T. Tan and S. H. Yeo, "Local POE model for robot kinematic calibration," *Mech. Mach. Theory* **36**, 1215–1239 (2001).
14. G. Chen, L. Kong, Q. Li, H. Wang and Z. Lin, "Complete, minimal and continuous error models for the kinematic calibration of parallel manipulators based on POE formula," *Mech. Mach. Theory* **121**, 844–856 (2018).
15. S. Xiang, H. Li, M. Deng and J. Yang, "Geometric error analysis and compensation for multi-axis spiral bevel gears milling machine," *Mech. Mach. Theory* **121**, 59–74 (2018).
16. Y. Zhao, T. M. Li and X. Q. Tang, "Geometric error modeling of machine tools based on screw theory," *Procedia Eng.* **24**(5), 845–849 (2011).
17. J. Yang, J. R. R. Mayer and Y. Altintas, "A position independent geometric errors identification and correction method for five-axis serial machines based on screw theory," *Int. J. Mach. Tools Manu.* **95**, 52–66 (2015).
18. T. Huang, H. T. Liu and D. G. Chetwynd, "Generalized Jacobian analysis of lower mobility manipulators," *Mech. Mach. Theory* **46**(6), 831–844 (2011).
19. H. Liu, T. Huang and D. G. Chetwynd, "A general approach for geometric error modeling of lower mobility parallel manipulators," *J. Mech. Robot.* **3**(2), 021013 (2011).
20. G. Prabhaharan, P. Asokan, P. Ramesh and S. Rajendran, "Genetic-algorithm-based optimal tolerance allocation using a least-cost model," *Int. J. Adv. Manuf. Tech.* **24**(9), 647–660 (2004).
21. T. Huang, D. G. Chetwynd, J. P. Mei and X. M. Zhao, "Tolerance design of a 2-DOF overconstrained translational parallel robot," *IEEE T. Robot.* **22**(1), 167–172 (2006).
22. A. Dumas, N. Gayton, J. Y. Dantan and B. Sudret, "A new system formulation for the tolerance analysis of overconstrained mechanisms," *Probabilistic Eng. Mech.* **40**(1), 66–74 (2015).
23. A. Goldsztejn, S. Caro and G. Chabert, "A New Methodology for Tolerance Synthesis of Parallel Manipulators," *Proceedings of the 14th World Congress in Mechanism and Machine Science*, Taipei, Taiwan (2015) pp. 132–141.
24. S. Caro, F. Bennis and P. Wenger, "Tolerance synthesis of mechanisms: A robust design approach," *ASME J. Mech. Design* **127**(1), 86–94 (2005).
25. K. W. Chase, W. H. Greenwood, B. G. Loosli and L. F. Hauglund, "Least cost tolerance allocation for mechanical assemblies with automated process selection," *Manuf. Rev.* **3**(1), 49–59 (1990).
26. A. Bensoussan, *Reliability* I*ndex, Optimal Control and Dynamic Games* (Springer, US, 2005), pp. 311–317.
27. T. Huang, C. Dong, H. Liu, X. Qin, J. P. Mei, Q. Liu and M. X. Wang, A novel 5-DOF hybrid robot with rotational supports, PCT/CN 2016/077464, 2016.03.28.
28. J. C. Tsai, F. C. Chen and J. H. Dai, "Reduction of tolerance stack-up by grouped random assembly for components with uniform distributions," *Procedia CIRP* **27**, 260–263 (2015).

Appendix

For the jth link ($j = 1, 2, \cdots, n$),

$$\hat{\$}_{1,j} = \begin{bmatrix} -a_j \hat{\boldsymbol{x}}_j \times \hat{\boldsymbol{z}}_{j-1} \\ \hat{\boldsymbol{z}}_{j-1} \end{bmatrix}, \hat{\$}_{2,j} = \begin{bmatrix} \hat{\boldsymbol{z}}_{j-1} \\ \boldsymbol{0} \end{bmatrix}, \hat{\$}_{3,j} = \begin{bmatrix} \hat{\boldsymbol{x}}_j \\ \boldsymbol{0} \end{bmatrix}, \hat{\$}_{4,j} = \begin{bmatrix} \boldsymbol{0} \\ \hat{\boldsymbol{x}}_j \end{bmatrix}$$

$$\hat{\boldsymbol{x}}_j = \begin{pmatrix} 1 \\ 0 \\ 0 \end{pmatrix}, \hat{\boldsymbol{z}}_{j-1} = \begin{pmatrix} 0 \\ \sin\varphi_j \\ \cos\varphi_j \end{pmatrix}$$

where $\hat{\boldsymbol{x}}_j(\hat{\boldsymbol{z}}_{j-1})$ is the nominal unit vector of the $x_j(z_{j-1})$-axis.

https://doi.org/10.1017/S0263574720000028 Published online by Cambridge University Press

For the end-link (the $(n+1)$th link),

$$\hat{\$}_{1,n+1} = \begin{bmatrix} -a_{n+1}\hat{\boldsymbol{u}} \times \hat{z}_n \\ \hat{z}_n \end{bmatrix}, \hat{\$}_{2,n+1} = \begin{bmatrix} \hat{z}_n \\ \mathbf{0} \end{bmatrix}, \hat{\$}_{3,n+1} = \begin{bmatrix} \hat{\boldsymbol{u}} \\ \mathbf{0} \end{bmatrix}, \hat{\$}_{4,n+1} = \begin{bmatrix} -d_e\hat{z}_{n+1} \times \hat{\boldsymbol{u}} \\ \hat{\boldsymbol{u}} \end{bmatrix},$$

$$\hat{\$}_{5,n+1} = \begin{bmatrix} \hat{z}_{n+1} \\ \mathbf{0} \end{bmatrix}, \hat{\$}_{6,n+1} = \begin{bmatrix} \mathbf{0} \\ \hat{z}_{n+1} \end{bmatrix}$$

$$\hat{z}_n = \begin{pmatrix} 0 \\ \sin\varphi_{n+1} \\ \cos\varphi_{n+1} \end{pmatrix}, \hat{z}_{n+1} = \begin{pmatrix} 0 \\ 0 \\ 1 \end{pmatrix}, \hat{\boldsymbol{u}} = \begin{pmatrix} \sin\theta_e \\ \cos\theta_e \\ 0 \end{pmatrix}$$

where $\hat{u}$ is the nominal unit vector of the x-axis in the transition frame (see Fig. 2).

https://doi.org/10.1017/S0263574720000028 Published online by Cambridge University Press